IMAV2018-48
http://www.imavs.org/pdf/imav.2018.48

Bio-inspired Regenerative Flight Trajectory Optimisation Over Flat Topography

N. K. Long*, and S. Watkins†
RMIT University, Plenty Rd, Bundoora VIC 3083, Australia
J.M. Moschetta‡, and V. Bonnin§
ISAE-SUPAERO, 10 Avenue Edouard Belin, Toulouse, 31400, France

ABSTRACT

A gliding technique, known as dynamic soaring (DS), replicates the flight pattern of albatross bird to enable energy-neutral, repeatable flight trajectories. This study investigated the potential for the flight manoeuvers of the albatross to act as a basis for UAV battery power regeneration by means of a windmilling propeller mounted on the aircraft. In order to give an indication of the type of atmospheric and environmental conditions necessary to perform regenerative dynamic soaring (RDS), trajectories were optimized for a small UAV. The optimal flight paths for varying amounts of energy regeneration and periodicity are presented and compared to a base, energy-neutral DS case. The findings suggest that by slightly altering the DS flight pattern, RDS is possible for both open- and closed-loop trajectories with significant battery recharge levels being reached for the UAV modelled under certain conditions.

1 INTRODUCTION

While unmanned flight vehicle technology continues to rapidly expand, new methods for extending their range and endurance are sought out. One solution was found by observing the way that wandering albatrosses (Diomedea Exulans) soar over the ocean seemingly effortlessly over distances exceeding 900km per day [1]. The technique the albatrosses use is known as dynamic soaring (DS). DS uses the vertical wind gradient, such as develops over the ocean in the case of the albatross, to enable energy neutral flight cycles comprised of four flight phases; a climb into the wind (1), a turn from windward to leeward flight direction (2), a descent with the wind (3), and a turn into the wind from leeward flight direction to windward (4) [2] (see Figure 1). By modelling the wind gradient as a logarithmic profile, Sachs was able to accurately simulate the flight pattern of the albatross, optimising the trajectory for minimum wind strength required [3]. Researchers then applied DS control algorithms to drone flight. As an example, Dietterl et al. simulated a small UAV flying DS trajectories while minimising the wind strength required, optimising for both open-loop and closed-loop flight paths [4]. Further, Langelaan discusses the potential for increasing small UAV range and endurance by extracting significant amounts of energy from the atmosphere via performing DS, in combination with other soaring techniques, by implementing a control algorithm which monitors atmospheric conditions in real-time [5].

Figure 1 gives an example simulation of the wandering albatross performing DS over a flat ocean. The four flight phases are numbered and colour coordinated, and the trajectory's two-dimensional (2D) projections are depicted on each plane. The orange arrow defines the direction of the wind profile.

Separately, a method for an aircraft to extract the power available in the wind and convert it into usable energy has been discussed in literature. Glauert was the first to examine the potential for placing a windmill on an aircraft [6]. MacCready then reintroduced a similar idea applied to a sailplane [7]. More recently, Barnes conducted a detailed analysis on the functioning of a dual-mode windmilling propeller capable of both generating thrust and extracting wind energy using regenerative braking technologies already employed on cars [8, 9]. The extracted energy was designed to then be stored on an onboard battery via a motor-generator. Bonnin et al. were the first researchers to optimise a flight trajectory for regenerative dynamic soaring (RDS), doing so on the leeward side of a hill where strong wind gradients are known to form [10]. Bonnin introduced a regenerative drag force (D_{gen}) to simulate the additional drag imparted on the aircraft when performing RDS, and optimised a closed-loop trajectory for the least wind strength required while fixing an average battery recharge rate (P_{net}).

This study aims to further the academic research on RDS by establishing the conditions required for RDS over a flat topography. Specifically, the effects of varying P_{net} on the wind strength required will be investigated with the hope of developing a greater understanding of how this effects the resulting trajectory and flight variables.

*Email addresses: *nathan.k.long.91@gmail.com, †simon@rmit.edu.au, ‡jean-marc.moschetta@isae.fr, §bonnin.v@gmail.com

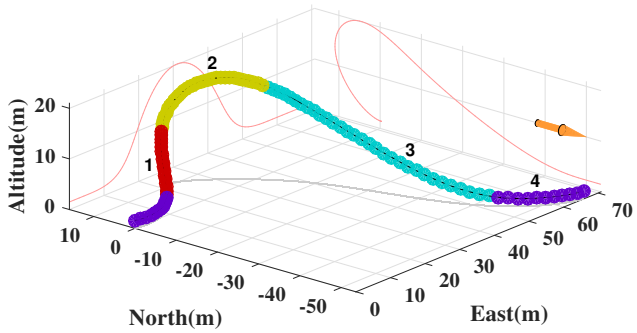

Figure 1: Albatross open-loop dynamic soaring trajectory simulation.

2 Methodology

2.1 Aircraft Model

The aircraft chosen for this study was the DT-18, a small UAV developed by Delair in Toulouse, France. The DT-18 was selected due to its slender body and relatively high aspect ratio (13.1), giving it a construction similar to the general structure of a wandering albatross which is known to have the highest aspect ratio of any living bird (16.8). Furthermore, the DS performance of the DT-18 was thoroughly investigated in Bonnin's doctoral dissertation [11], and used for the RDS optimisation on the leeward side of a hill completed by Bonnin et al. [10].

The aircraft has been represented as a point-mass so as to reduce the complexity of the model and permit a higher degree of abstraction for any conclusions. This point represents the centre of gravity whereby all forces are assumed to act upon it, and bank angle (ϕ) is the only rotation permitted about it.

2.2 Wind Model

Various models have been used to approximate the vertical wind gradient (or wind shear) that develops within the boundary layer over a flat surface, however, Sachs [2], Barnes [9, 8], and Bonnin [11] chose to implement a logarithmic profile for their DS simulations. This decision was based on the flight altitude of the albatross, and on the wind strengths required for DS. One major flaw of this wind profile approximation is its neglect of turbulence-related unsteadiness which would undoubtedly have an effect on the flight dynamics of an aircraft flying within it, however, for the purpose of this study it has been deemed acceptable. Equation 1 gives relationship between the wind strength (V_w) along the logarithmic profile and altitude (z).

$$V_w = U_{ref} \cdot \frac{\ln(z/z_0)}{\ln(z_r/z_0)} \tag{1}$$

Equation 1 also details the reliance on a reference wind height (z_r) and reference wind speed (U_{ref}) in developing the wind profile. A reference wind height of $10m$ was used throughout this study, the same as used by Sachs for his DS study [2]. Furthermore, Equation 1 portrays the effect of surface roughness length (z_0) on the wind profile. A value of $20cm$, representing a flat suburban topography, was fixed for this study in order to focus on the effects of P_{net} on the wind profile and RDS flight variables. The effects of obstacles on the wind profile and trajectories have been assumed negligible. A separate study by Long et al., investigating the effects of surface roughness on RDS flight trajectories, has been **submitted** for publication [12].

2.3 Kinetics, Kinematics, and Thermodynamics

DS has been analysed via both the inertial frame of reference and wind-based frame of reference [13], however, the inertial frame of reference has been selected for the following RDS optimisation as it seems more intuitive to comment on the results based on their ground-relative performance. Based on the inertial reference frame assumption, Sachs et al. argue that the fundamental energy gain experienced during DS is during the turn from upwind to downwind [3].

The coordinate system used for the trajectory mapping is such that the x-axis aligns with north, y-axis with east, and negative z-axis with positive altitude. The relationship between the airspeed vector (V_a) and ground speed vector (V_i), and their associated heading angles (ψ), flight path angles (γ)[1], and ϕ, with respect to the coordinate system are outlined in Bonnin's thesis [11]. Equation 2 then highlights how V_i, V_a and V_w are related.

$$V_a = \sqrt{V_i^2 - 2V_iV_w\cos\psi_i\cos\gamma_i + V_w^2} \tag{2}$$

The system state variables, which define the dynamic state of the aircraft and describe its evolution along a flight trajectory, are V_i, ϕ_i, γ_i, x, y, and z. The control variables, which govern the state variables and are considered manipulable by the aircraft control system or pilot, are the lift coefficient (C_L), ϕ, and the regenerative drag force (D_{gen}) acting on the windmilling propeller.

Figure 2 portrays how D_{gen} is added to the forces acting upon the DT-18 (actual representation of a DT-18 side-view).

Equations 3 to 6 define the force equations for the aircraft system, where the additional drag force (D_{gen}) is of particular interest. It should be noted that D_{gen} then has a subsequent effect on the equations of motion and, thus, the evolution of the aircraft's trajectory. The formulation of the equations of motion is identical to those used by Bonnin [11].

$$\vec{F}_{ext} = F_x\vec{x} + F_y\vec{y} + F_z\vec{z} \tag{3}$$

$$F_x = -L(\sin\phi\sin\psi_a + \cos\phi\cos\psi_a\sin\gamma_a) - (D + D_{gen})(\cos\gamma_a\cos\psi_a) \tag{4}$$

$$F_y = L(\sin\phi\cos\psi_a - \cos\phi\sin\psi_a\sin\gamma_a) - (D + D_{gen})(\cos\gamma_a\sin\psi_a) \tag{5}$$

[1] Subscript a is used to represent air-based variables, and subscript i is used to represent ground-based / inertial variables.

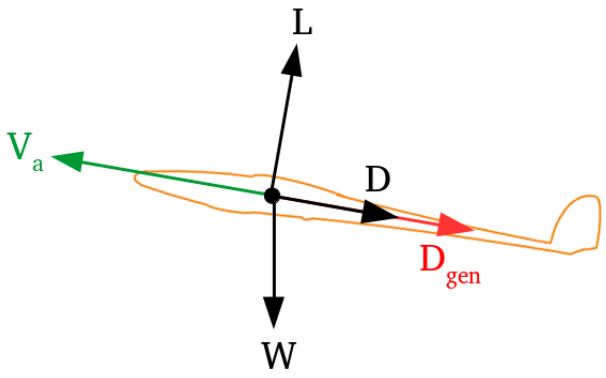

Figure 2: Forces acting on DT-18 UAV developed by Delair (reproduced from Long et al.[12]).

$$F_z = -L\cos\phi\cos\gamma_a + (D + D_{gen})(\sin\gamma_a) + mg \quad (6)$$

RDS requires a series of power conversions in order for the aerodynamic power (P_{aero}) imparted onto the windmilling propeller, defined in Equation 7, to recharge the onboard battery, in Equation 8. This causes efficiency losses to occur and, as such, a fixed efficiency (η_{regen}) of 0.6 is applied to P_{aero} to represent the losses across the entire power chain before entering the battery. This efficiency was based on mimicking the efficiency used in the RDS study by Bonnin et al. [10].

$$P_{aero} = -\vec{D}_{gen} \cdot \vec{V}_a \quad (7)$$

$$P_{gen} = \dot{E}_{bat} = (\vec{D}_{gen} \cdot \vec{V}_a)\,\eta_{regen} \quad (8)$$

$$P_{net} = \frac{\Delta E_{bat}}{t_{cycle}} \quad (9)$$

The net power income (P_{net}), given in Equation 9, represents the average battery recharge rate experienced during one RDS flight cycle. P_{net} is used as a benchmark for the amount of power available for harvesting along a defined RDS trajectory.

2.4 Optimisation Setup

The trajectories presented in this study have been optimised by using the Sparse Nonlinear OPTimizer (SNOPT) solver available on the NEOS server. SNOPT takes first-order derivatives as input defined by a specific structure. A Mathematical Programming Language (AMPL) was, thus, used to convert the equations of motion, variable constraints, and objective function into the format required by SNOPT. A MATLAB script coupled to the SNOPT-AMPL package was used as the interface for the data input and output. SNOPT converges on a local optimum solution and, therefore, a large range of input parameters was required to validate the results. The entire setup was replicated from Bonnin's DS trajectory optimisation research [11], and a list of exact constraints for the optimisation can be found within his dissertation. In summary, a series of bounds are placed on the aircraft system which are set to ensure that the resulting trajectories were realistic and physically feasible. Periodicity is also applied as a final condition whereby the variable (z, γ, ψ, ϕ, C_L, V_i, and D_{gen}) final conditions must equate their initial conditions. For the closed-loop optimisations, x and y periodicity was also constrained.

The solver is given an objective function which defines a variable or parameter to either maximise or minimise by manipulating the state and control variables while complying with the constraints and adhering to the equations of motion. As DS is highly dependent on the wind gradient present, the objective function was set to minimising the reference wind speed at a reference height of $10m$ for this study. Identifying the wind strengths required for RDS while varying P_{net} values will help to expand knowledge on the environmental conditions necessary for RDS to be achieved. Furthermore, minimising U_{ref} at $10m$ matches Sachs' optimisation setup [2], and was validated by Bonnin [11] with his setup by using an albatross as the vehicle model and comparing his results to those of Sachs. Differences in results were found to be minor, with a maximum 2% variation found for the variables and parameters tested (U_{ref}, t_{cycle}, Δx_{max}, Δy_{max}, and Δz_{max}).

3 Results and Discussion

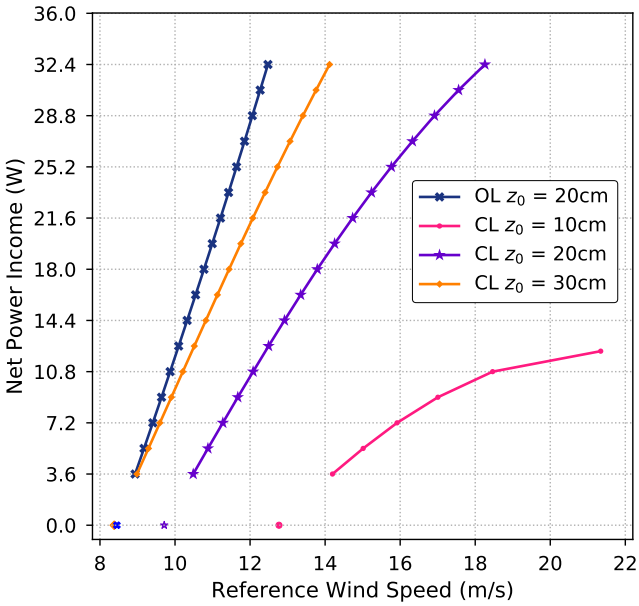

Figure 3: RDS reference wind speed vs. net power income (adapted from Long et al. [12]).

A range of P_{net} values were tested with a fixed surface roughness length of $20cm$ to establish the conditions needed to generate more power during flight.

Figure 3 shows the trends for the U_{ref} required for an enforced P_{net} for both open- and closed-loops. The open-loop

trajectory for a surface roughness of $20cm$ is represented by the blue line, requiring the lowest wind strength to permit RDS. The U_{ref} needed was found to increase linearly as P_{net} was increased. The linear relation existed for a closed-loop trajectory over a rougher surface ($z_0 = 30cm$, depicted in orange), however, at a surface roughness of $20cm$ (in purple) the linear trend became distorted at a P_{net} of approximately $18W$, though the aircraft was still able to regenerate the full range of P_{net} values tested. Reducing the surface roughness further to $10cm$ saw a complete breakdown of the linear trend, and an inability of the aircraft to fly closed-loop trajectories beyond a P_{net} value of approximately $13W$. The open-loop RDS trajectory trends were shown to be completely linear down to a surface roughness of $3cm$ [12]. Hereafter, the results from three rates of P_{net}, $10.8W$, $21.6W$, and $32.4W$, are presented alongside the pure DS case for $z_0 = 20cm$.

3.1 Open-Loop Regenerative Dynamic Soaring

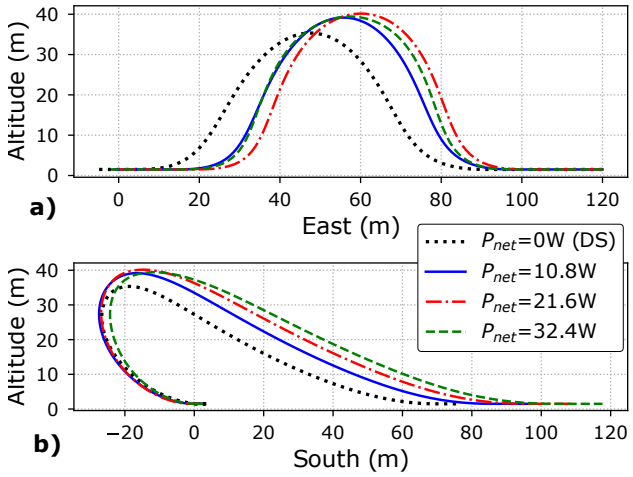

Figure 4: Open-loop 2D trajectories for: a) west-east displacement, and b) north-south displacement.

The west to east displacement (Figure 4a) for the varying P_{net} values, while not following exactly the same paths, were very similar. The DS case, however, significantly varied from the others. The differences between the RDS cases is likely be attributed to SNOPT finding local optimum solutions, not caused by any physical phenomenon. Each trajectory reached an altitude of approximately $40m$ and displaced approximately $120m$ east. The DS case, however, flew to a lower altitude, climbing sooner, and not displacing as far east. This could be explained by the fact that the DS constraints were such that it did not require energy regeneration, only to continue flying, so did not have to climb to reach higher wind strengths.

The comparison of north to south movement shows a further displacement south for higher P_{net} values, and an increase in altitude upon decent.

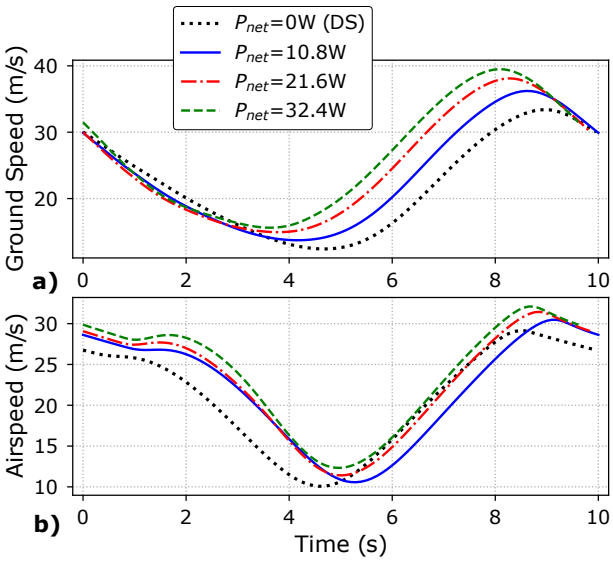

Figure 5: Time versus: a) ground speed. b) airspeed.

Taking the results from Figures 4, and 5a and b together, the further displacement south during descent gave a higher inertial speed, which resulted in a higher airspeed, allowing for the additional power generation (seen in Equation 7).

Figure 6a describes the evolution of D_{gen} during flight. As P_{net} is increased, D_{gen} shifts from being applied only during the descent (as with the $P_{net} = 10.8W$ case) to also being applied during the upper turn from windward direction to leeward direction. As P_{net} is increased the amount of force applied during the upper turn is increased, even surpassing the amount applied during the descent for higher recharge rates (Figure 6a). The maximum airspeeds achievable during decent for the aircraft must be reached whereby no further drag can be accrued, therefore, the aircraft must begin extracting energy during the upper turn. As outlined by Sachs et al. [3], when describing the energy evolution of an aircraft performing DS in the inertial frame, the principal gain in energy is at the top of the trajectory due to the change in orientation of the ground speed vector. Applying extra drag force at the top of the trajectory could be attributed to the fact that the potential energy of the aircraft is high at this point, and with no further power required to ascend or fly windward, the system could afford to convert some of the energy into electricity. The battery recharge rate (P_{gen}) for the $P_{net} = 32.4W$ and $P_{net} = 21.6W$ cases reach their maximum during the descent so, although a higher D_{gen} is applied during the upper turn, a much higher airspeed is seen during descent (Figure 5a).

Figure 6a shows D_{gen} non-dimensionalised with respect to the drag force required for powered straight and level (S&L) flight for maximum endurance by the DT18. D_{gen} ratios are between 60% and 120% of the $S\&L$ aerodynamic

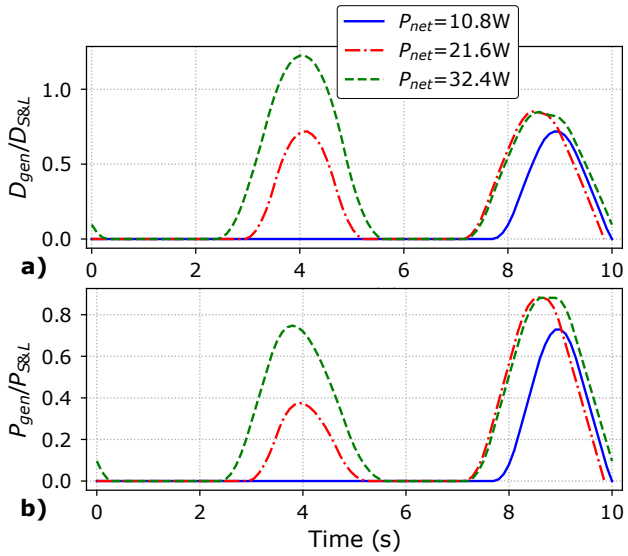

Figure 6: Time versus non-dimensionalised: a) regenerative drag force. b) battery recharge rate.

drag force. Figure 6b gives the variation of P_{gen} with time and has been non-dimensionalised with respect to the power expenditure experienced during maximum endurance $S\&L$ flight. The amount of regenerative power available for harvesting reaches levels close to the same amount of the power required to fly $S\&L$.

3.2 *Closed-Loop Regenerative Dynamic Soaring*

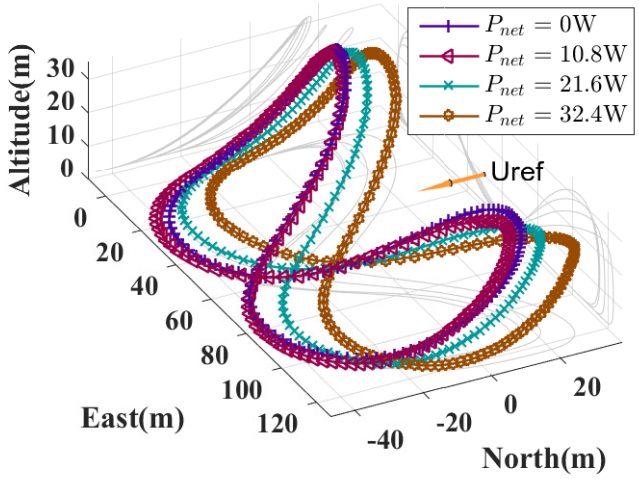

Figure 7: Closed-loop RDS trajectories for varying P_{net} values.

The closed-loop RDS trajectories all followed the same pattern, a recreation of the four DS flight phases which were then mirrored and flown in the reverse direction to form a continual loop. Analyzing the 2D projections in Figure 7 shows that there was a decrease in altitude, a shift upwind, and a increase in the cross-wind displacement for the trajectories with a higher P_{net}. The orange arrow represents the reference wind height and the direction of the wind vector.

As opposed to the open-loop RDS power regeneration, the closed-loop cases harvested no power during the leeward descent; all of the power is regenerated during the upper turns from windward to leeward direction. This could be due to the fact that the aircraft needed to conserve its kinetic energy from the descent to turn back into the wind and climb again without any net displacement with the wind.

4 Conclusion

The investigation into the effects of increasing P_{net} on RDS flight trajectories showed that, for a higher P_{net}, a greater area for displacement was required. Furthermore, for the open-loop RDS trajectories, power harvesting shifted from only during flight descent for lower P_{net} values, to also occurring during the upper turn for higher P_{net} values. On the other hand, the closed-loop trajectories extracted power from the wind only during the upper turns from windward flight to leeward flight, and the trajectories experienced a general flattening for higher levels of P_{net}.

Future studies into RDS should focus on the inclusion of thrust augmentation to test how a combined windmilling propeller would affect the RDS flight trajectories. The model should also be elaborated to investigate how the aerodynamic performance of different windmilling propellers will affect RDS performance, and further refinement of the wind profiles should be incorporated into RDS optimisations to represent the effects of obstacles and local unsteadiness.

Acknowledgements

The authors would like to express their appreciation for the Department of Aerodynamics, Energetics and Propulsion (DAEP) at ISAE-SUPAERO for their support and funding of this research, and to RMIT University for their input and backing of the project. A special thanks would like to be given to Dr Thierry Jardin and Yuchen Leng at the DAEP for their regular advice and assistance throughout the study, as well as to Dr Abdulghani Mohamed at RMIT for his encouragement and guidance.

References

[1] S. M. Waugh, P. A. Prince, and H. Weimerskirch. Geographical variation in morphometry of black-browed and grey-headed albatrosses from four sites. *Polar Biology*, 22(3):189–194, 1999.

[2] G. Sachs. Minimum shear wind strength required for dynamic soaring of albatrosses. *Ibis*, 147(1):1–10, 2005.

[3] G. Sachs, J. Traugott, A. P. Nesterova, F. Kummeth, W. Heidrich, A. L. Vyssotski, and F. Bonadonna. Fly-

ing at no mechanical energy cost; disclosing the secret of wandering albatross. *PLoS One*, 7(9), 2012.

[4] M. Deittert, A. Richards, C. A. Toomer, and A. Pipe. Engineless unmanned aerial vehicle propulsion by dynamic soaring. *Journal of Guidance, Control, and Dynamics*, 32(5):1446–1457, 2009.

[5] J. W. Langelaan. Power generation and energy management. *Encyclopedia of Aerospace Engineering*, pages 1–20, 2016.

[6] H. Glauert. *The elements of aerofoils and airscrew theory*. Cambridge University Press, Cambridge, United Kingdom, 1926.

[7] P. MacCready. Regeneratve battery-augmented soaring. *Technical Soaring*, 23(1):28–32, 1999.

[8] P. J. Barnes. Aircraft energy gain from an atmosphere in motion: dynamic soaring and regen-electric flight compared. 2015.

[9] P. J. Barnes. Regenerative electric flight: Synergy and integration of dual-role machines. In *53rd AIAA Aerospace Sciences Meeting*, 2015.

[10] V. Bonnin, E. Benard, and J-M. Moschetta. Energy-harvesting by dynamic soaring on the leeward side of a hill. 2016.

[11] V. Bonnin. *From albatrosses to long range UAV flight by dynamic soaring*. PhD thesis, 2015.

[12] N. K. Long, S. Watkins, J.M. Moschetta, and V. Bonnin. Regenerative dynamic soaring trajectory augmentation over flat terrains. to appear.

[13] D-N. Liu, Z-X. Hou, Z. Guo, X-X. Yang, and X-Z. Gao. Bio-inspired energy-harvesting mechanisms and patterns of dynamic soaring. *Bioinspiration Biomimetics*, 12(1):016014, 2017.